Adsorption kinetics behavior of MB dye on CaO nanosheets

A. Modwi[a], M. A. Aissa[a], A. I. Alakhras[b,c], H. Idriss[c,d,*]
[a]*Department of Chemistry, College of Science and Arts, Qassim University, Al-Rass 51921, Saudi Arabia*
[b]*Chemistry Department, College of Science, Imam Mohammad Ibn Saud Islamic University (IMSIU), Riyadh 13318, Saudi Arabia*
[c]*Physics Department, College of Science, Imam Mohammad Ibn Saud Islamic University (IMSIU), Riyadh 13318, Saudi Arabia*
[d]*Deanship of Scientific Research, Imam Mohammad Ibn Saud Islamic University (IMSIU), Riyadh, Saudi Arabia*

The work reported herein demonstrates the fabrication of CaO nanosheets employing a thermal decomposition method. The obtained CaO nanosheets were characterized using TEM, BET, XRD, EDX, and FTIR instruments. Moreover, the effect of initial dye concentration and pH on MB removal by CaO nanosheets was studied. The result showed that the nanoparticles have sizes around 100 nm, and the CaO nanosheets have an average diameter of 50 nm. Meanwhile, the average pore diameter and surface area of CaO are 15.847 Å and 5.881 m2. g^{-1}, respectively. Numerical models based on Temkin, Freundlich, and Langmuir were applied to adsorption data to better understand the MB dye adsorption onto CaO nanoparticles. The sorption findings demonstrated a stronger fit with the Temkin model (R^2 = 0.983) compared to the Freundlich model (R^2 = 0.947) and Langmuir model (R^2 = 0.968). The maximum adsorption capacity of MB on the CaO nanoparticles is 688.01 mg/g. The investigation determined that the adsorption kinetics adhered to the Pseudo-second-order kinetic model(R^2=0.982).

(Received October 25, 2023; Accepted January 22, 2024)

Keywords: CaO, nanosheets, Adsorption, MB dye, Kinetics, Isotherms

1. Introduction

Water shortage is one of the most serious problems that our planet is currently dealing with [1, 2], and it is becoming increasingly severe. The world population is predicted to reach over 40 percent by 2050, with over 40 percent of the world's population living in areas of serious water scarcity [2]. The inexorable reduction in the quality and availability of drinking water is unquestionably a result of the expanding population of the world and the unsustainable industrial expansion that has taken place in recent decades [3-9]. Water is polluted by the inevitable discharge of industrial wastewater, containing a wide variety of non-biodegradable, dangerous inorganic, and organic impurities such as pesticides, heavy metals, cosmetics, dyes, medications, and other substances [10-13]. Among all these toxins, dyeing sewage discharged by various enterprises has resulted in visibly severe water pollution. Due to the exceptionally high color strength, it affects the clarity of the water, increasing the level of organic substances in bodies of water [14-16].

Numerous techniques have been employed to remove organic dyes from industrial effluents, including solvent extraction [17], chemical precipitation [18], ion exchange [19], electrochemical treatment [20], membrane processes [21], and adsorption processes [22]. Adsorption is a particularly interesting method for eliminating contaminants from aqueous systems due to its excellent dependability [23-28]. While many grades of commercially available materials with a high surface area continue to be widely available, they are prohibitively expensive. Due to this result, there is an increasing need for lead adsorption adsorbents that are reasonably effective,

* Corresponding author: hiidriss@imamu.edu.sa
https://doi.org/10.15251/JOR.2024.201.93

affordable, and widely available, particularly when the adsorbents are wastes. The researchers concentrated on low-cost adsorbents synthesized in a straightforward manner with lowering chemical reagents used [29]

2. Methodology

2.1. *CaO nanosorbent* fabrication and characterization

Thermally decomposing carbonate salts created calcium oxide (CaO) nanoparticles. Two grams of calcium carbonate salts were weighed, placed in a crucible, and annealed at 1073 K for one hour.

Calcium oxide CaO nanosheets were generated, chilled to room temperature, and employed for MB removal characterization and application. Several scientific and spectroscopic methodologies were employed to describe the CaO nanosorbent. X-ray diffraction (XRD) was employed to evaluate the phase composition and crystallinity using a Bruker D8 advance diffractometer in the two supplied with Cu-K (λ = 1.540) radiation reference. The ASAP 2020 apparatus was used to analyze the surface quality (HD88 micrometrics). Fourier-transformed infrared (FTIR) spectra were acquired before and post MB dye removal using a Nicolet 5700 spectrometer and a KBr. Scanning electron microscopy (SEM) with a Hitachi S4700 and transmission electron microscopy (TEM) with a Tecnai G20 running at 200 kV exciting voltage were used to analyze the surface morphology. Energy dispersive X-ray (EDX) spectroscopy was utilized to analyze the elemental composition of manufactured CaO. The concentration of MB dye was evaluated using a spectrophotometer device.

2.2. MB adsorption procedure

To calculate the adsorption rate of MB dye onto CaO nanosheets, two kinetic models were used: pseudo-first-order (PFO) and pseudo-second-order (PSO). These models incorporate adsorbed quantities after adsorption of MB dye as function of time, which enables us to determine the reaction kinetics

3. Results and discussion

3.1. CaO nanosorbent characterizations

The experiments investigated the morphologies of CaO nanoparticles fabricated from calcium carbonite. TEM images of CaO nanoparticles synthesized at various scales are shown in Fig. 1(a-c). The TEM images found that the nanoparticles have an almost **sheets**-like shape and a uniform size. Furthermore, the nanoparticles are evenly dispersed with a narrow size distribution. The nanoparticles have sizes around 100 nm, and the CaO nanosheets have an average diameter of 50 nm. The findings agree with the size determined by the Debye-Scherrer equation in XRD measurements, indicating that the nanoparticles are monocrystalline. EDX spectra were used to determine the elemental composition of the obtained nanomaterials. The EDX spectra revealed the presence of oxygen (O) and calcium (Ca), with no impurities (Fig. 1d). The constituents of the CaO nanomaterial are determined by Energy-Dispersive X-ray Spectroscopy (EDX). Therefore, it is evident from the results of EDX of CaO nanomaterial that the surface consists of oxygen (O) and calcium (Ca), as the spectrum corresponds to these constituents, as given in Figures 1f-g.

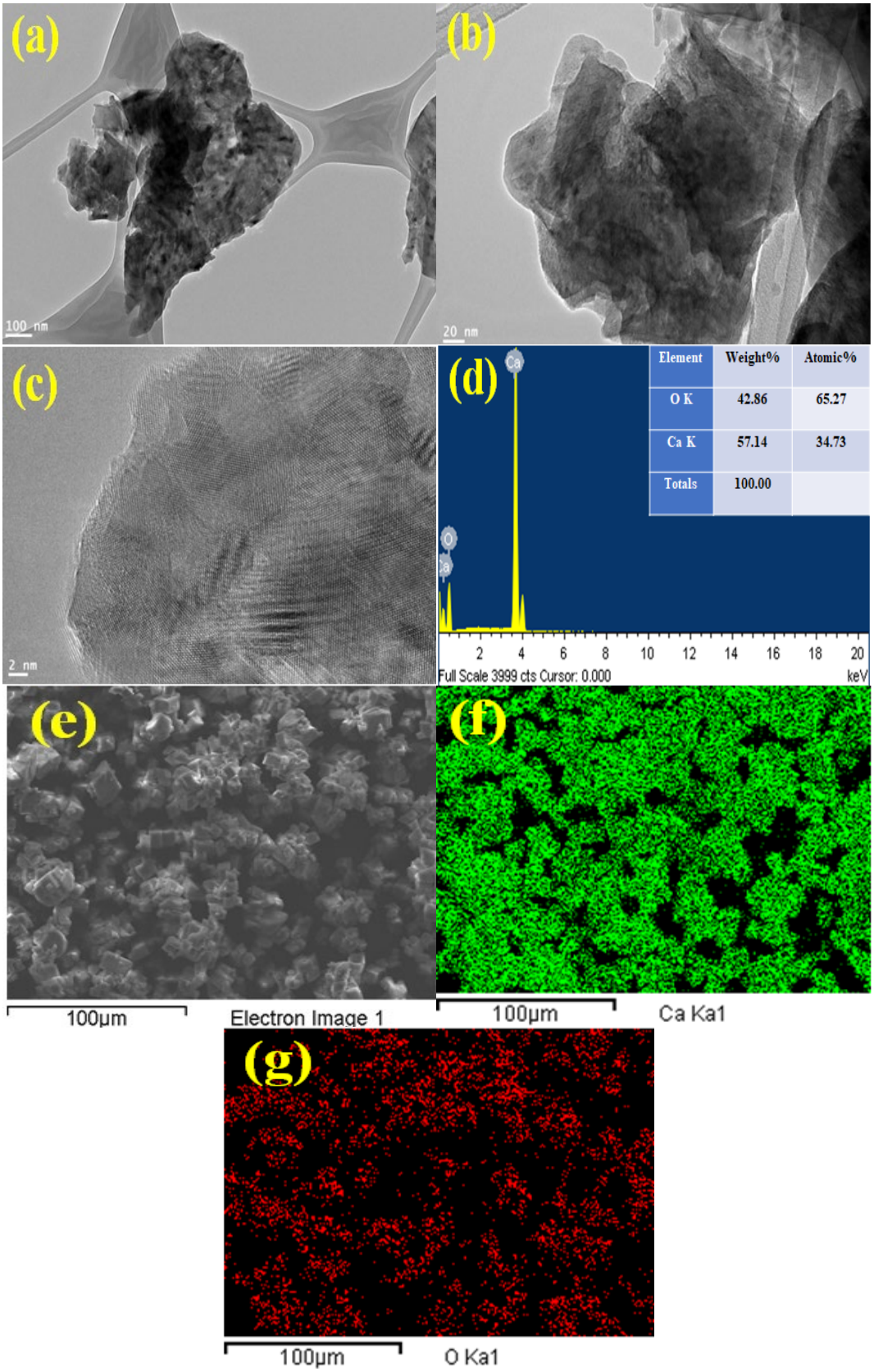

Fig. 1. TEM images with different magnifications (a-c), EDX graph (d), and elemental mapping distribution (e-g) of CaO nanosheets.

The chemical bonding and composition of the produced CaO were determined by FTIR analysis, as shown in Fig. 2a. The stretching vibration of the O-H group is allocated to a broad band at 3665 cm^{-1} in FTIR spectra [30]. In contrast, the -OH stretching mode of the adsorbed water molecule is assigned to a band at 1655 cm^{-1}. Furthermore, the three bands detected at 1533, 1402, and 1056 cm^{-1} are associated with an unidentified carbonate adsorbed on the surface of nanoparticles [31]. The characteristic band located at 872 cm^{-1} is assigned to Ca-O stretching vibration mode [32].

The XRD pattern of CaO (Fig.) reveals peaks 2θ ≈ 32.07, 37.27, 53.80, 64.04 and 67.23° which are related to the (110), (200), (202), (311) and (222) planes of the crystal cubic phase of *CaO* [XRD file JCPDS No. 77-2376] [33]. In addition, a $CaCO_3$ small peak is observed at 47.28 and 48.37° beside the CaO peaks. The presence of calcite ($CaCO_3$) demonstrates the incomplete pyrolysis of the precursor and / or rapid carbonation and hydrolysis of the formed CaO by atmospheric CO_2 and moisture. Literature reported the high potential of CaO nanoparticles for trapping greenhouse gas CO_2 [34].

N_2-sorption measurements were used to examine the textural features of CaO nanosheets (Fig. 2c). The nitrogen adsorption isotherm profiles show typical Type III behavior patterns, characteristic of microporous materials, while the non-limited increase of adsorbed N_2 at P/P0 values around 0.5 reveals free monolayer-multilayer sorption that may be related to the presence of inter-particle porosity [35]. This phenomenon might be due to the occurrence of non-rigid aggregates of nanoparticles shape [36]. Furthermore, the hysteresis loop on the majority of isotherms implies the presence of tiny holes (such as mesopores) inside the sample [37, 38]. Fig. 2d presents the pore size distributions of the fabricated CaO sorbent. The average pore diameter and surface area of CaO are found to be 15.847 Å and 5.881 $m^2 . g^{-1}$, respectively.

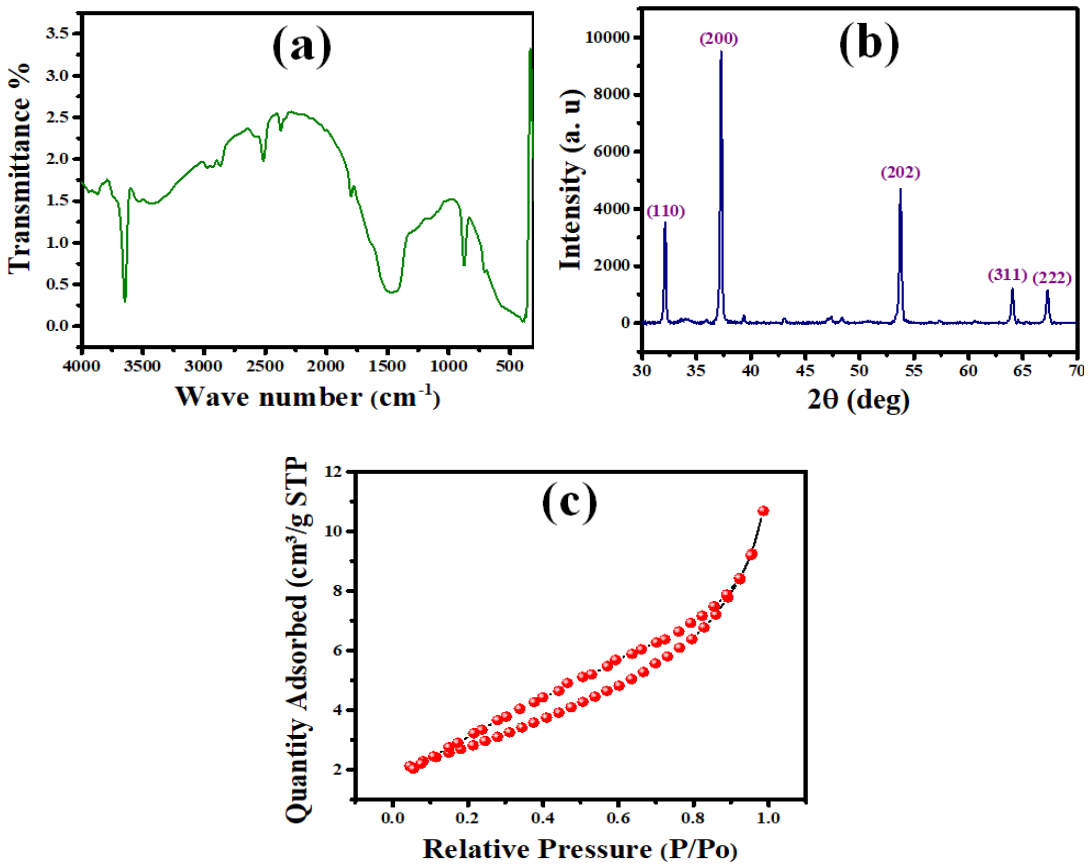

Fig. 2 (a) FTIR spectra, (b) XRD patterns, and (c) Nitrogen adsorption-desorption isotherm of CaO nanosheets.

3.2. MB removal onto CaO nanosheets

3.2.1. Impact of initial dye concentration and pH on MB removal by CaO nanosheets

The influence of initial dye concentration on CaO nanosheet adsorption ability was investigated. Based on starting dye concentrations ranging from 10 to 200 mg/L, the adsorption capacity of MB increased from 17.55 to 380.75 mg/g, as shown in Fig. 3 a. These data suggest that increasing the initial dye concentration not only improves the quantity of dye adsorption onto the fixed dose of adsorbent but also increases competition among dye molecules on the limited active sites of the adsorbent. Furthermore, increasing the initial dye concentration enhances the remaining dye concentration in the solution. Because dye adsorption is also dependent on the adsorbent's adsorption active site composition.

CaO nanosheets as-prepared were used to study the influence of pH on cationic MB adsorption ability. In general, the pH of the adsorption system has a substantial effect on the interaction between the dye molecule and the sorbate and, consequently, on the adsorption capacity of the adsorbent. Hence, the influence of the initial pH of the dye solution on the adsorption of CaO nanosheets towards MB was initially investigated. Due to their dissimilar electronegativity, as demonstrated in Fig. 3 b, the MB adsorption capabilities exhibited opposing fluctuation tendencies. At starting pH ranging from 3 to 11, the MB sorption rose dramatically from 3.24 to 167.33 mg/g. When the pH was adjusted to 12, an adsorption capacity of 22.46 mg/g was recorded.

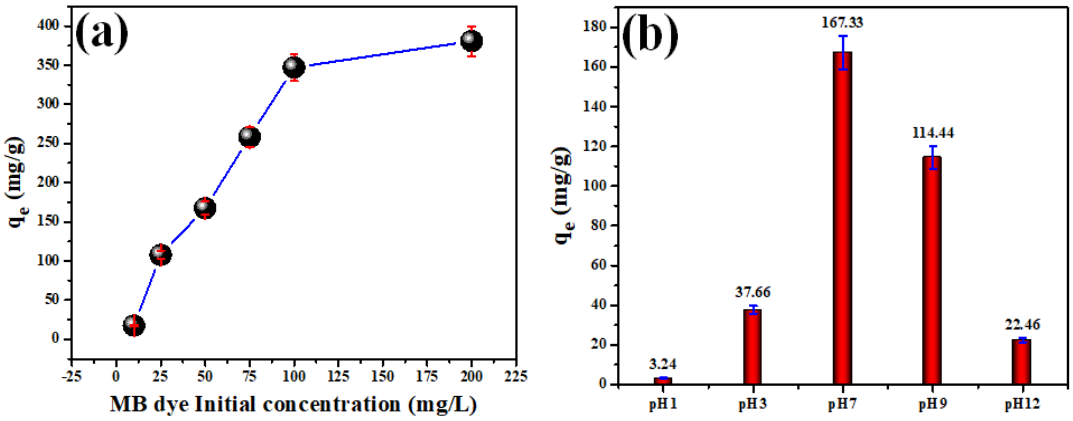

Fig. 3. (a) Influence of the initial MB concentration at pH = 7 and (b) impact of pH on the MB adsorption capacity.

3.2.2. Adsorption isotherms

Temkin, Freundlich, and Langmuir's isotherm models were applied to the adsorption data to better understand the process of MB dye adsorption onto CaO nanoparticles and to estimate the optimal adsorption efficiency manifested by nanoparticles for varying MB concentrations. The non-linear formulas of the applied isotherms are shown in Table 1.

Table 1. Isotherm constants for MB dyes adsorption onto CaO nanoparticles.

Isotherm		Parameter	Values
Langmuir	$q_e = \frac{q_{max} K_L C_e}{1 + K_L C_e}$	q_m (mg. g^{-1})	688.01
		K_L (mg. g^{-1})	0.027
		R_L (L.mg^{-1})	0.546
		R^2	0.968
Freundlich	$q_e = k_F C_e^{1/n}$	1/n	0.660
		K_F (L.mg^{-1})	31.256
		R^2	0.947
Temkin	$q_e = B_T ln C_e A_T$	B_T(J.mol^{-1})	136.79
		A_T (L.mg^{-1})	0.328
		R^2	0.983

Figures 3 (a-c) depicts the nonlinear fitting isotherm model for MB dye adsorption into CaO NPs. The sorption results (Table 1) fit better to the Temkin model (R^2 = 0.983) than to the Freundlich model (R^2 = 0.947) and Langmuir model (R^2 = 0.968). The maximal MB adsorption capacity on the CaO NPs is 688.01 mg. g^{-1}. According to the authors' best knowledge, this value is greater than other adsorbents employed for MB removal. Numerous adsorbents have been used in the literature to eliminate MB dye, with their adsorption capacity frequently falling below the value determined in this study. Table 2 shows the elimination efficiencies of CaO NPs and a few adsorbents from the scientific literature.

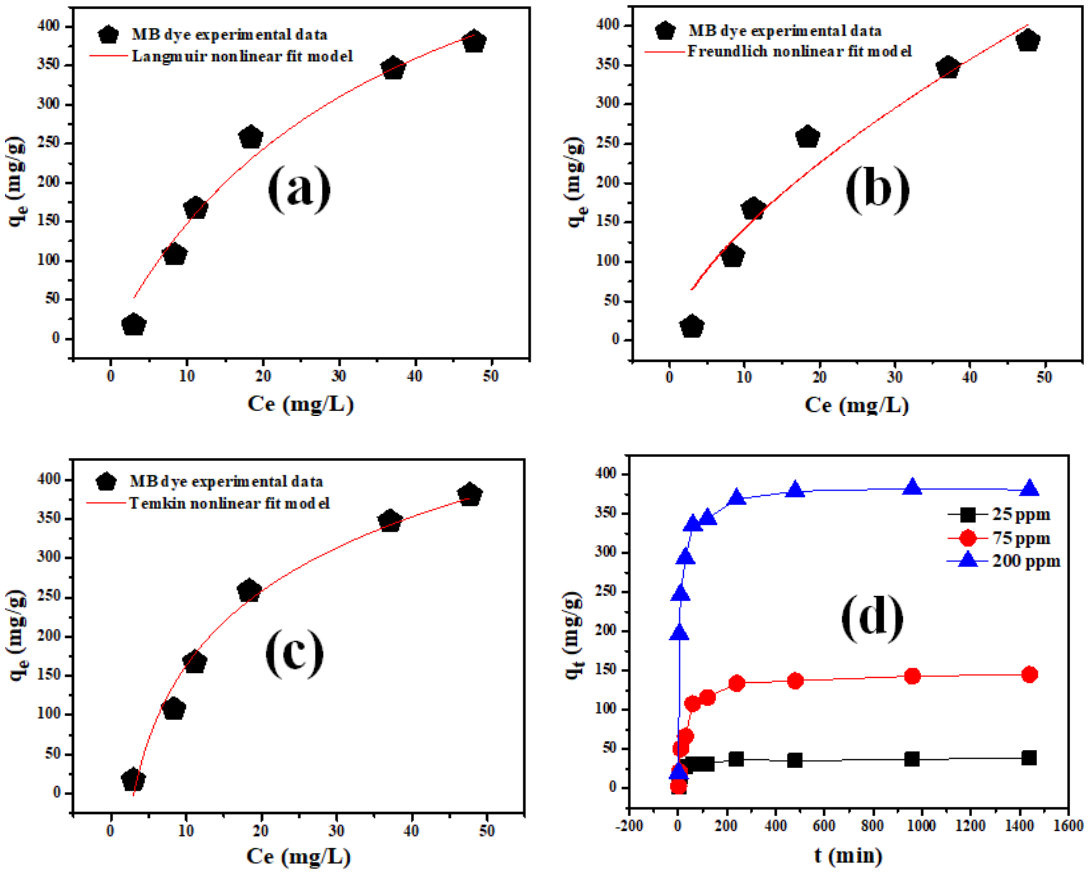

Fig. 4. MB adsorption equilibrium data fitted using Langmuir(a), Freundlich (b), Temkin (c), and (d) contact time effect on the MB adsorption rate onto CaO nanosheets.

Table 2. Sorption capability of some sorbents for the Pb (II) metal ions removal.

Adsorbents	Adsorption capacity ($mg.g^{-1}$)	Contact time (min)	Ref.
polymeric natural carbohydrate of turmeric	157.33	180	[39]
GO@CA	369.85	30	[40]
COFs	315.6	-	[41]
Desalted duck egg	166.67	60	[42]
BMP gel	361.9	20	[43]
porous silica	303	-	[44]
CaO	688.01	7	This work

3.2.3. Time effect and adsorption Kinetics

The adsorption capabilities of CaO nanosheets (0.5 g/L) against MB as a function of contact time were examined. Fig. 5 demonstrates that the MB adsorption capabilities varied; however, their fluctuation patterns were comparable as the contact duration increased. At the initial 60 min, the sorption rates of CaO nanosheets towards MB were rapid, and their respective adsorption capacities were around 28.33, 132.89 and 358.49 mg/g. After that, the MB adsorption capabilities of CaO nanosheets exposed to dye solutions for extended periods rose steadily until reaching a peak. The equilibrium adsorption capacity was around 378.92 mg/g for 200 ppm initial MB concentration, indicating that CaO nanosheets preferentially absorb cationic MB in the ambient pH environment. The formation of a dye molecular layer on the surface of CaO nanosheets likely contributed to the dye molecules' resistance to sorption.

Non-linear models were fitted to experimental data to understand CaO nanosheets adsorption dynamics toward MB. Table 3 displays the associated computed parameters. When compared to the pseudo-first-order model, the pseudo-second-order model showed a higher coefficient (R^2) value 0.983 for MB adsorption. Fig. 5b showing how the pseudo-second-order kinetic model for MB adsorption onto CaO nanosheet fits the data better. Further, the measured q_e exp value agrees with the equilibrium adsorption capacity, q_e cal, of MB obtained from the pseudo-second-order fitted plot (Fig. 5b and Table 3).

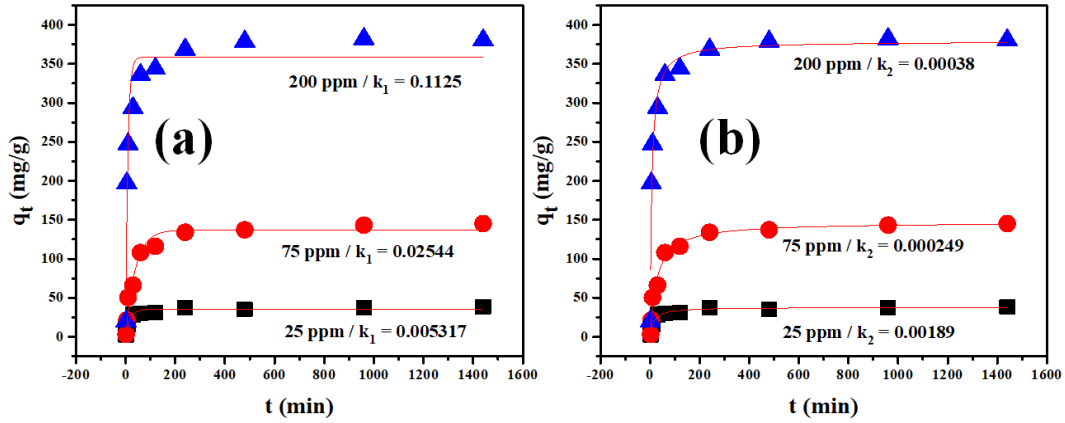

Fig. 5. (a) PFO and (b) PSO for MB removal on prepared CaO nanosorbent.

Table 3. Computed adsorption kinetic parameters for MB elimination onto CaO.

Kinetics Model		Parameter	25 ppm	75 ppm	200 ppm
Pseudo-first-order	$\ln(q_e - q_t) = \ln q_e - k_1 t$ [45]	q_e	35.37	137.01	358.52
		K_1	0.005317	0.02544	0.1125
		R^2	0.967	0.964	0.908
Pseudo-second-order	$\frac{t}{q_t} = \left[\frac{1}{k_2 q_e^2}\right] + \frac{1}{q_e} t$ [45]	q_e	37.77	146.96	378.92
		K_2	0.00189	0.000249	0.00038
		R^2	0.982	0.983	0.936

3.3. Adsorption mechanism

Several parameters, including the type of the adsorbate, the functional groups on the adsorbents and dyes, the solution pH, the surface charge on the nanomaterial, and so on, could influence the adsorption mechanism. To further elucidate the process of MB adsorption onto CaO Nps, the

FTIR spectrum before adsorption are compared to the MB@CaO spectrum. The FTIR spectrum of pure MB shows several characteristic bands. For example, the bands at 2816 cm^{-1} for C−H stretching of methyl groups, and 1591 to 1363 cm^{-1} for C=C stretching of the aromatic ring structures. Comparing the spectrum of CaO before and after adsorption reveals that some characteristic MB bands have shown up and shifted relative to those of the free MB molecules.

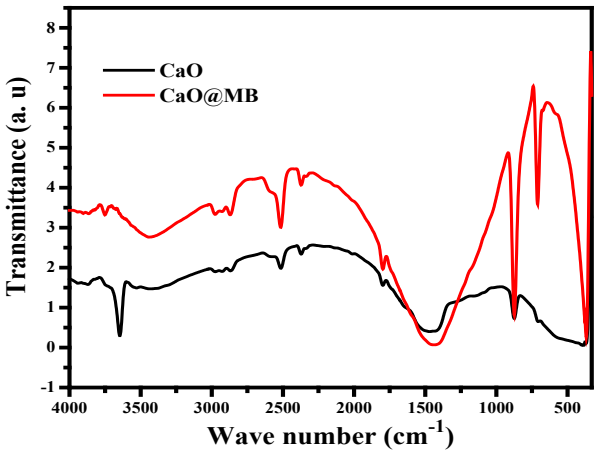

Fig. 6. FTIR spectra of CaO before and after MB adsorption.

4. Conclusion

The study concluded that the prepared calcium oxide (CaO) nanosheets demonstrated optimistic characteristics and premium efficacy in eliminating methylene blue (MB) dye from aqueous solutions. The obtained CaO nanosheets have sizes around 100 nm and an average diameter of 50 nm. Furthermore, the average pore diameter and surface area of CaO are 15.847 Å and 5.881 $m^2. g^{-1}$, respectively. As a result of the sorption results, the Temkin model (R^2 = 0.983) provided a stronger fit than either the Freundlich (R^2 = 0.947) or Langmuir models (R^2 = 0.968). The CaO nanoparticles exhibit a maximum adsorption capacity of 688.01 mg/g for MB. According to data analysis, the adsorption kinetics is consistent with a pseudo-second-order kinetic model (R^2=0.982).

Acknowledgements

The authors extend their appreciation to the Deanship of Scientific Research, Imam Mohammad Ibn Saud Islamic University (IMSIU), Saudi Arabia, for funding this research work through Grant No. (221412017).

References

[1] Mashkoor, F., A. Nasar, C. Jeong, Biomass Conversion and Biorefinery, 2022: p. 1-13; https://doi.org/10.1007/s13399-021-02282-3

[2] Novais, R.M., et al., Journal of Cleaner Production, 2018. 171: p. 783-794; https://doi.org/10.1016/j.jclepro.2017.10.078

[3] Kant, R., Textile dyeing industry an environmental hazard. 2011; https://doi.org/10.4236/ns.2012.41004

[4] Nasar, A., RSC advances, 2014. 4(108): p. 62844-62850.

[5] Zhao, F., et al., Journal of colloid and interface science, 2013. 409: p. 174-182; https://doi.org/10.1016/j.jcis.2013.07.062

[6] Modwi, A., et al., Environmental Research, 2022. 205: p. 112543; https://doi.org/10.1016/j.envres.2021.112543

[7] Khezami, L., et al., Biochemical Engineering Journal, 2022: p. 108411; https://doi.org/10.1016/j.bej.2022.108411

[8] Khezami, L., et al., Ceramics International, 2022. 48(4): p. 5805-5813; https://doi.org/10.1016/j.ceramint.2021.11.128

[9] Toghan, A., A. Modwi, Journal of Photochemistry and Photobiology A: Chemistry, 2021. 419: p. 113467; https://doi.org/10.1016/j.jphotochem.2021.113467

[10] Nasar, A., Chemical Papers, 2014. 68(1): p. 65-73; https://doi.org/10.2478/s11696-013-0424-7

[11] Ippolito, A., G. Fait, Current opinion in environmental sustainability, 2019. 36: p. 78-84; https://doi.org/10.1016/j.cosust.2018.10.023

[12] Elamin, M.R., et al., Molecules, 2022. 28(1): p. 176; https://doi.org/10.3390/molecules28010176

[13] Modwi, A., et al., Inorganics, 2022. 10(11): p. 210; https://doi.org/10.3390/inorganics10110210

[14] Uddin, M.K., et al., Materials Research Bulletin, 2021. 139: p. 111279; https://doi.org/10.1016/j.materresbull.2021.111279

[15] Rahali, S., et al., Langmuir, 2021. 37(24): p. 7285-7294; https://doi.org/10.1021/acs.langmuir.1c00378

[16] Baaloudj, O., et al., Materials, 2021. 14(18): p. 5409; https://doi.org/10.3390/ma14185409

[17] Liu, W., et al., Algal Research, 2022. 64: p. 102656; https://doi.org/10.1016/j.algal.2022.102656

[18] Li, Y., et al., Chemosphere, 2022. 296: p. 134033; https://doi.org/10.1016/j.chemosphere.2022.134033

[19] Joseph, J., et al., Materials Chemistry and Physics, 2020. 242: p. 122488; https://doi.org/10.1016/j.matchemphys.2019.122488

[20] Ghalkhani, M., et al., Food and Chemical Toxicology, 2022: p. 112830; https://doi.org/10.1016/j.fct.2022.112830

[21] Januário, E.F.D., et al., Chemical Engineering and Processing-Process Intensification, 2021. 168: p. 108577; https://doi.org/10.1016/j.cep.2021.108577

[22] Modwi, A., et al., Zeitschrift für Naturforschung A, 2018. 73(11): p. 975-983; https://doi.org/10.1515/zna-2018-0219

[23] Ngoc, P.K., et al., Journal of Science: Advanced Materials and Devices, 2022. 7(2): p. 100438; https://doi.org/10.1016/j.jsamd.2022.100438
[24] Wang, Z., et al., Separation and Purification Technology, 2022: p. 120838; https://doi.org/10.1016/j.seppur.2022.120838
[25] Aldaghri, O., et al., Science of The Total Environment, 2024. 906: p. 167685; https://doi.org/10.1016/j.scitotenv.2023.167685
[26] Modwi, A., et al., Inorganic Chemistry Communications, 2023: p. 111594; https://doi.org/10.1016/j.inoche.2023.111594
[27] Aissa, M.A.B., et al., Inorganics, 2023. 11(4): p. 146; https://doi.org/10.3390/inorganics11040146
[28] Modwi, A., A. Albadri, and K.K. Taha, Diamond and Related Materials, 2023. 132: p. 109698; https://doi.org/10.1016/j.diamond.2023.109698
[29] Abdulkhair, B.Y., et al., Zeitschrift für Naturforschung A, 2019. 74(10): p. 937-944; https://doi.org/10.1515/zna-2019-0059
[30] Xu, S., et al., Environmental research, 2020. 186: p. 109489; https://doi.org/10.1016/j.envres.2020.109489
[31] Wu, P.-Y., et al., New Journal of Chemistry, 2016. 40(3): p. 2878-2885; https://doi.org/10.1039/C5NJ02358K
[32] Margaretha, Y.Y., et al., International Journal of Energy and Environmental Engineering, 2012. 3(1): p. 1-9; https://doi.org/10.1186/2251-6832-3-33
[33] Madhu, B., et al., Structural, SN Applied Sciences, 2021. 3(6): p. 1-7; https://doi.org/10.1007/s42452-021-04607-3
[34] Mirghiasi, Z., et al., Journal of industrial and Engineering chemistry, 2014. 20(1): p. 113-117; https://doi.org/10.1016/j.jiec.2013.04.018
[35] Degirmenbasi, N., et al., Fuel, 2015. 153: p. 620-627; https://doi.org/10.1016/j.fuel.2015.03.018
[36] Thommes, M., et al., Reinoso, J. Rouquerol, KSW Sing, Pure and applied chemistry, 2015. 89(9-10): p. 1051-1069; https://doi.org/10.1515/pac-2014-1117
[37] Hosseini, S.G., et al., Powder Technology, 2015. 278: p. 316-322; https://doi.org/10.1016/j.powtec.2015.03.032
[38] Sing, K.S., Pure and applied chemistry, 1985. 57(4): p. 603-619; https://doi.org/10.1351/pac198557040603
[39] Kubra, K.T., M.S. Salman, M.N. Hasan, Journal of Molecular Liquids, 2021. 328: p. 115468; https://doi.org/10.1016/j.molliq.2021.115468
[40] Eltaweil, A.S., et al., Journal of Porous Materials, 2023. 30(2): p. 607-618; https://doi.org/10.1007/s10934-022-01347-6
[41] Hsu, Y.-C., et al., Applied Surface Science, 2023. 612: p. 155890; https://doi.org/10.1016/j.apsusc.2022.155890
[42] Wang, Y., et al., Journal of Molecular Liquids, 2023: p. 121210; https://doi.org/10.1016/j.molliq.2023.121210
[43] Zhang, X., et al., Gels, 2023. 9(1): p. 40; https://doi.org/10.3390/gels9010040
[44] Subhan, F., et al., Inorganic Chemistry Communications, 2022. 139: p. 109380; https://doi.org/10.1016/j.inoche.2022.109380
45. Lagergren, S.K., Vetenskapsakad. Handingarl, 1898. 24: p. 1-39.